AFRL-SN-RS-TR-2003-49
Final Technical Report
March 2003

DEVELOPMENT OF A COMPACT, LOW JITTER MODELOCKED SEMICONDUCTOR DIODE LASER

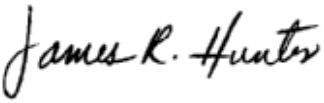**University of Central Florida**

APPROVED FOR PUBLIC RELEASE; DISTRIBUTION UNLIMITED.

AIR FORCE RESEARCH LABORATORY
SENSORS DIRECTORATE
ROME RESEARCH SITE
ROME, NEW YORK

This report has been reviewed by the Air Force Research Laboratory, Information Directorate, Public Affairs Office (IFOIPA) and is releasable to the National Technical Information Service (NTIS). At NTIS it will be releasable to the general public, including foreign nations.

AFRL-SN-RS-TR-2003-49 has been reviewed and is approved for publication.

APPROVED: *James R. Hunter*

JAMES R. HUNTER
Project Engineer

FOR THE DIRECTOR: *Richard G. Shaughnessy*

RICHARD G. SHAUGHNESSY, Lt Col, USAF
Chief, Rome Operations Office
Sensors Directorate

REPORT DOCUMENTATION PAGE

Form Approved
OMB No. 074-0188

1. AGENCY USE ONLY (Leave blank)	2. REPORT DATE	3. REPORT TYPE AND DATES COVERED
	MARCH 2003	Final Jul 99 – Jul 02

4. TITLE AND SUBTITLE
DEVELOPMENT OF A COMPACT, LOW JITTER MODELOCKED
SEMICONDUCTOR DIODE LASER

5. FUNDING NUMBERS
C - F30602-99-1-0546
PE - 62204F
PR - 4600
TA - SN
WU - 02

6. AUTHOR(S)
Peter J. Delfyett

7. PERFORMING ORGANIZATION NAME(S) AND ADDRESS(ES)
University of Central Florida
CREOL Building, PO Box 162700
4000 Central Florida Blvd
Orlando Florida 32816-2700

8. PERFORMING ORGANIZATION REPORT NUMBER

9. SPONSORING / MONITORING AGENCY NAME(S) AND ADDRESS(ES)
Air Force Research Laboratory/SNDP
25 Electronic Parkway
Orlando Florida 32816-2700

10. SPONSORING / MONITORING AGENCY REPORT NUMBER

AFRL-SN-RS-TR-2003-49

11. SUPPLEMENTARY NOTES

AFRL Project Engineer: James R. Hunter/SNDP/(315) 330-7405/ James.Hunter@rl.af.mil

12a. DISTRIBUTION / AVAILABILITY STATEMENT
APPROVED FOR PUBLIC RELEASE; DISTRIBUTION UNLIMITED.

12b. DISTRIBUTION CODE

13. ABSTRACT *(Maximum 200 Words)*
This research project was aimed at generating a train of ultralow noise optical pulses from a semiconductor diode laser for applications in optical sampling. Typical optical sampling applications may be similar to that encountered in analog to digital converter scenarios. The performance parameters aimed for in this project would support 12 bits of effective resolution at a sampling rate of 10 gigasamples per second. The results of this effort show that by properly engineering the modelocked oscillator design, the timing stability of modelocked diode lasers may perform on a par of atomic clocks.

14. SUBJECT TERMS
Optic, Digital Converter, Modelocked Oscillator, Diode Laser

15. NUMBER OF PAGES
35

16. PRICE CODE

17. SECURITY CLASSIFICATION OF REPORT	18. SECURITY CLASSIFICATION OF THIS PAGE	19. SECURITY CLASSIFICATION OF ABSTRACT	20. LIMITATION OF ABSTRACT
UNCLASSIFIED	UNCLASSIFIED	UNCLASSIFIED	UL

Table of Contents

List of Figures

Goal:

The purpose of this research contract is to develop a compact, modelocked semicondutor diode laser that possesses suitable output characteristics for applications in a 10 Gsps, 10-12 bit optical sampling photonic analog to digital converter.

The overall operation specifications is to show the following:

- Relative amplitude stability of 0.01%
- Relative timing jitter of less than 50 fsec
- Temporal pulse duration of less than 2 picoseconds
- Pulse repetition frequency of 10 GHz.

Since the program has begun, we have successfully demonstrated the following:

- Low amplitude noise of 0.1% @ 10 GHz (10 Hz-10 MHz).
- Low timing jitter of 43 femtoseconds at 10 GHz (10 Hz-10 MHz).
- Pulse duration of 1.2 psec @ 10 GHz (1.7 times transform limit assuming Gaussian pulse shapes)
- Operation at 1.55 microns
- Nonlinear measurements (absorption) of multiple quantum well saturable absorbers via the Z- scan method.
- Initial development of a novel jitter measurement using optical interferometry.
- Development of a dielectric coating procedure for depositing anti-reflection coatings on semiconductor multiple quantum well saturable absorbers.
- Demonstration of optical sampling streams at 80 Gigasamples per second.
- Performed a detailed survey on the amplitude timing jitter of the modelocked laser varying the following: 1) pulse repetition frequency, 2) modulation technique (gain or loss), 3) synthesizer noise.
- Development of a phase lock loop to assist in reducing timing jitter (operating at 2 GHz; demonstrated a 91% in phase noise 10 Hz- 100kHz; 88 fsec to 8 fsec)
- Demonstration of a fundamentally modelocked diode laser at 10 GHz (pulse duration 4 psec).
- First demonstration ever of passive modelocking of diode laser using 1550 multiple quantum well saturable absorbers.
- Demonstration of the measured integrated phase noise sidebands to Nyquist (5 GHz,), showing noise contributions of the modelocked diode laser, RF amplifiers, and noise measurement floor.
- Complete characterization of both AM and PM noise (integrated to 5 GHz) of a *fundamentally* modelocked laser clock operating at 10 Gsps.
- Complete characterization of both AM and PM noise (integrated to 5 GHz) of a *harmonically* modelocked laser clock operating at 10 Gsps.

- Demonstration of the contribution **_(conclusive proof)_** of supermode noise to the residual timing jitter (phase noise) of modelocked optical clocks.

- Demonstration of the lowest phase and amplitude noise characteristics achieved to date using active harmonic modelocking in an external-cavity semiconductor diode ring laser (35 fsec, 10 Hz to 10 MHz).

- Demonstration of wideband supermode suppression utilizing a high-finesse fiber-Fabry-Perot intracavity etalon.

- Measurement results on the residual phase noise knee position and as a function of laser cavity frequency for a hybridly modelocked external linear cavity semiconductor laser.

- Measurement results on the longitudinal mode linewidth as a function of laser cavity frequency for a hybridly modelocked external linear cavity semiconductor laser.

- Demonstration of the knee position and the average linewidth of the individual modelocked longitudinal modes are directly correlated with each other.

- Demonstration of the average linewidth of the individual modelocked longitudinal modes can be measured by using residual noise measurement techniques,

- Demonstration that the limits of RMS pulse-to-pulse timing jitter is determined by the linewidth of the modelocked longitudinal modes.

Results &Conclusion

The results of this project successfully demonstrated the performance of a semiconductor modelocked diode laser system with output characteristics compatible for optical sampling applications requiring ~10 bits of effective resolution. A key result of this works clearly identifies a limiting mechanism that directly determines the performance characteristic of a semiconductor modelocked laser. By properly engineering the modelocked oscillator design, we predict that the timing stability of modelocked diode lasers may perform on a par of atomic clocks.

<u>**INTRODUCTION**</u>

This final report is organized into four (4) major sections:

1) the development of an ultralow noise external cavity actively modelocked ring diode laser,

2) an extension of the RF phase noise measurement method out to offset frequencies of 5 GHz, and conclusive evidence of the contribution of supermode noise to RF phase noise and timing jitter,

3) the invention of a novel method to completely suppress supermode noise, resulting in an integrated timing jitter of 18 fsec, which is to our knowledge the lowest timing jitter ever achieved in an actively modelocked semiconductor diode laser, and

4) the observation that a major fundamental limiting phenomena in the reduction in the timing jitter lies in the reduction in the optical longitudinal mode linewidth.

<u>Section 1</u>

In this section, we report on the development of an ultralow-noise, external-cavity, actively modelocked semiconductor diode laser for application in next-generation photonic sampling systems. A summary of harmonically-modelocked noise characteristics in a 65 MHz ring cavity is presented through the range of pulse repetition frequencies between 130 MHz and 8.3 GHz (2nd through 128th harmonic). Important implications regarding the use of gain- versus loss-modulation as the active modelocking mechanism are discussed. We also report what are, to our knowledge, the lowest noise characteristics achieved to date for a semiconductor diode laser operating at 10 GHz. Measured results of 0.12% RMS amplitude noise (10 Hz-10 MHz), and 43 fs RMS residual phase jitter (10 Hz-10 MHz), each obtained in an optimized configuration, provide a theoretical resolution of 8.6 bits in a 10 GSPS optical analog-to-digital converter. We have also achieved dispersion-compensated pulsewidths as short as 1.2 ps, and shown successful operation of a novel phase-locked-loop capable of reducing the RMS residual phase noise by as much as 91%. Finally, the first measurements of residual phase noise out to the Nyquist frequency (5 GHz) are presented, providing an upper bound on the RMS residual phase jitter of 121 fs (10 Hz-5 GHz).

1.1 Introduction

The notion of using optical pulsetrains to sample temporal signals for analog-to-digital conversion has been around for several decades, prompted by the recognition of the considerably greater bandwidth and low wideband dispersion available in the optical domain [1]. Published results using purely electronic analog-to-digital converters (ADCs) have shown a capability of ~3-6 bits of digital resolution at 8-10 GHz sampling rates [2-4] for analog bandwidths equal to half the sampling rate. The desire to further increase both bit resolution and sampling rates has inspired the active investigation of several possible approaches [5-16].

It should be mentioned here that commercially available digitizing oscilloscopes exist, operating at 20 Gsps with 8 bit of resolution. It should be noted however, that these systems use oversampling and time-interleaved techniques which minimize the analog bandwidth to be sampled, e.g., 3 GHz. Also, the overall clock performance in these commercial systems is ~10x lower compared to the optical sampling clock describe in this work. The key issue is that the limitation on the accuracy of any high speed sampling scheme will be determined by the clock accuracy.

While many of these strategies show promise, the primary limitations on the accuracy of any high-speed sampling scheme will be determined by noise characteristics [17].

As a foundation for highly accurate clocking and sampling in a next-generation optical ADC, we propose an actively-modelocked external-cavity semiconductor diode ring laser, capable of producing ultralow-noise pulsetrains with repetition rates as high as 20 GHz and pulsewidths as short as 1.2 ps. Experimental investigations of the noise characteristics of this laser form the backbone of this report.

The purpose of this report is to bring together the broad range of noise effects and techniques for their measurement and control based one laser system. The wide range of experimental results of the noise properties of modelocked lasers based on laser systems with greatly varying operating conditions makes it difficult for researchers to perform a fair comparison. This work, by addressing the broad range of issues, provides researchers a framework by which to assess and compare the noise characteristics of modelocked diode lasers over a broad range of operating conditions, e.g. repetition rate, oscillator noise, etc.

The report is organized as follows: The experimental architecture will be discussed in section II. This is followed in section III by a comparative survey of laser noise characteristics as a function of both modelocking frequency (cavity harmonic number) and modelocking technique (gain- versus loss-modulation). Noise and pulsewidth characteristics during highly-optimized operation at 10 GHz are presented in section IV, along with a proof-of-principle demonstration (at 2 GHz) of residual phase noise reduction through the use of a novel phase-locked-loop. Finally, the implications of extended noise sideband measurements out to Nyquist offset frequencies (5 GHz) are discussed in section V.

1.2 Experimental Geometry
A and peripherals is shown in Figure 1.1. The oscillator ring cavity (longitudinal mode spacing ~ 65 MHz) consists of a 2.3 mm InGaAsP semiconductor optical amplifier (SOA) and a fiber-pigtailed Mach-Zehnder intensity modulator. The ring is made to be unidirectional by the insertion of two intracavity Faraday isolators. An etalon (FSR ~7 nm, finesse ~ 5) is inserted in the cavity to limit the modelocked bandwidth and achieve lowest noise operation. Although broadband multiwavelength pulsetrains have previously been demonstrated using these laser systems [18, 19], the present geometry is implemented in a narrowband, single-wavelength form in order to eliminate the possibility of additional noise due to interwavelength modegroup competition [20]. The etalon is later removed to allow the modelocked spectrum to broaden for shortest-pulse operation, resulting in slightly higher levels of RMS noise. Following the oscillator, a second SOA provides single-pass amplification, after which the pulsetrain is directed

either to a high-speed photodiode (BW ~20 GHz) for noise measurement or to a dual-grating compressor for dispersion compensation/pulsewidth measurement. The ~10 dB of optical loss in the dispersion-compensator necessitates further amplification via EDFA before pulsewidths are measured using a standard SHG autocorrelator.
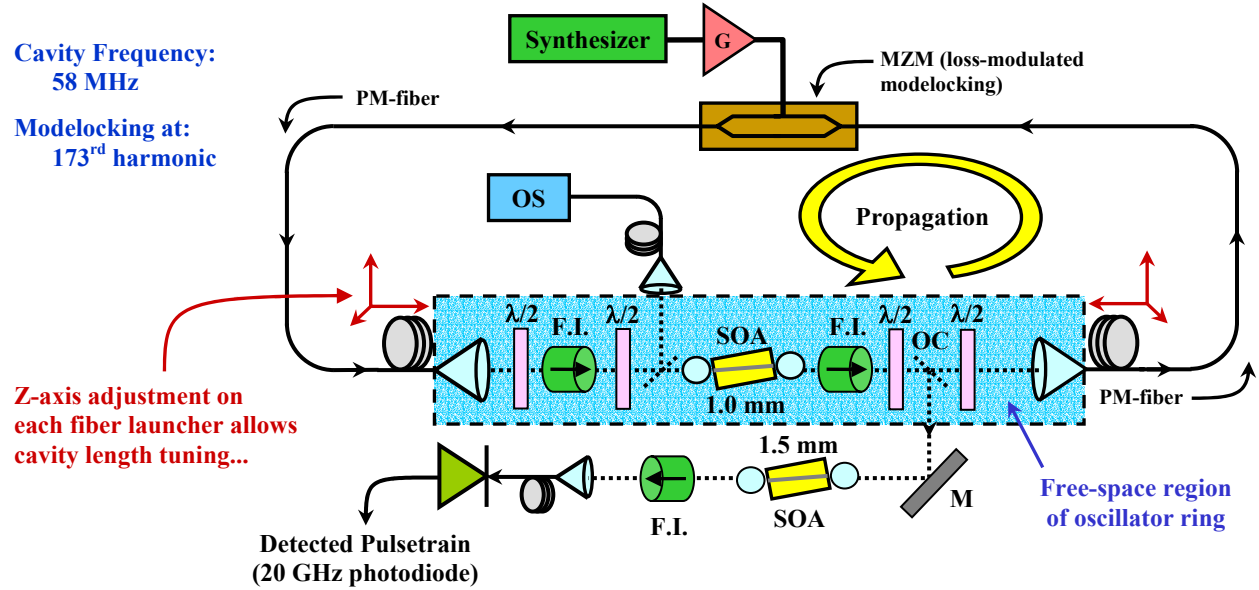
Fig. 1.1 Experimental configuration of the modelocked diode laser system.

Modelocking was achieved using two techniques: loss modulation and gain modulation. Loss modulation involved biasing the SOA at 90-120 mA DC (depending on modelocking frequency) while applying a synthesized RF sine wave (+25 dBm) to the Mach-Zehnder modulator. Gain-modulated modelocking required a lower DC bias on the SOA (80-95 mA) while the RF signal (+30 dBm) was injected into the SOA through a bias tee. Current data consists of actively-modelocked pulse rates as high as 10 GHz using loss-modulation, and 1 GHz using gain modulation (the gain-modulated frequency response was limited to 1 GHz by the impedance characteristics of the diode and mount).

Pulsetrain phase noise results were acquired by mixing the low-pass-filtered fundamental frequency component of the detected optical signal with that of the driving synthesizer (thereby translating the carrier noise sidebands down to baseband) [21]. The noise signals were then amplified and resolved over six decades of offset frequency (10 Hz-10 MHz) with a HP 3585A RF spectrum analyzer. Amplitude noise sidebands were similarly resolved in the frequency domain after being isolated from phase noise through a Shottky-diode detector in a HP 11729C Carrier Noise Test Set.

1.3 General Survey of Ring Laser Noise
Due to its traveling wave nature, the unidirectional ring cavity allows easy access to the technique known as harmonic modelocking. In an effort to better understand the laser's noise characteristics, a survey of noise data was compiled at octave intervals of the modelocking frequency, beginning with operation at the 2nd cavity harmonic (130 MHz) and ending with the

128th (8.32 GHz). Two driving synthesizers were used—a very low-noise HP 8663A (100 kHz - 2.5 GHz) as well as a high-frequency HP 83712B (10 MHz - 20 GHz). In addition, the laser was actively modelocked using loss modulation as well as gain modulation, and the effects of the two techniques on pulsetrain noise are compared. Although gain-modulated modelocking of the 2.3 mm SOA was only possible for frequencies up to ~1 GHz due to system impedance limitations in the instrumentation, some useful insight can nevertheless be gained from the resulting data.

It should be noted that there exists several oscillators that can outperform the 8663A, noting however the single-frequency output of these oscillators. The nature of these experiments require an RF source with a wide range of frequency tuning and as a result provide valuable information for a one-to-one comparison, even when using a less-than-optimal source.

Three classes of noise were investigated: amplitude modulation (AM) noise, as well as both "absolute" and "residual" phase modulation (PM) noise. Absolute PM noise, in this case, is used to refer to the situation in which the laser's detected pulsetrain was referenced to a synthesizer having significantly lower noise characteristics (8663A) than the one driving the laser (83712B). Measurements of absolute PM noise were made only when the 83712B was providing the laser's driving signal, since no source exists with significantly lower-noise than the 8663A. Residual PM noise refers to a comparison between the detected optical signal and the synthesizer signal actually driving the laser, and therefore could be measured using both sources. Residual noise represents the phase noise added to the driving signal by the laser cavity. All three noise types were measured over six decades of offset frequency (10 Hz-10 MHz), and the data points in the following figures represent the result of integration over this entire range. It should be noted that the general trends that will be identified in Figures 1.2, 1.3 and 1.4 are independent of integration band. The expressions used to calculate RMS values for timing jitter and amplitude noise follow from [21] and [22] respectively.

$$\Delta t_j = \frac{1}{2\pi \cdot f_c} \sqrt{2 \int_{f_{lo}}^{f_{hi}} L(f) \, df} \qquad (1)$$

$$\frac{\Delta a}{A} = \sqrt{2 \int_{f_{lo}}^{f_{hi}} P_A(f) \, df} \qquad (2)$$

Equation (1) indicates the RMS timing jitter, Δt_j, (in units of seconds) as a function of the RF carrier frequency, f_c, and the single-sideband phase noise density, $L(f)$ (measured relative to the carrier power). Equation (2) indicates the RMS amplitude fluctuation, $\Delta a/A$, (units are in percent relative to the average RF carrier power, A) as a function of the single-sideband amplitude noise density, $P_A(f)$. Noise densities in both equations are integrated over offset frequencies between f_{lo} and f_{hi}. In Figures 3 and 4 that follow, the results of phase noise integrations are also plotted in relative units (percent of the carrier period, T) so as to normalize the comparison between different modelocking frequencies:

$$\frac{\Delta t_j}{T} = \frac{1}{2\pi} \sqrt{2 \int_{f_{lo}}^{f_{hi}} L(f) \, df} \qquad (3)$$

6

It should be noted that supermode noise has been ignored in the integration, owing to the unresolved issue as to whether these components primarily affect AM or PM noise. Most importantly, the suppression of supermode noise to −140 dBc/Hz recently been demonstrated, which negates the need of their inclusion in the integration of noise (See Section 3).

The results of the noise survey are shown in Figures 1.2, 1.3 and 1.4, where the integrated and normalized (units of %) RMS noise is plotted versus modelocking frequency for each combination of driving synthesizer and modelocking method. Figures 1.2, 1.3 & 1.4 show the amplitude noise, residual phase noise, and absolute phase noise, respectively, each plotted versus modelocking frequency. In all three plots, the dotted curves with open symbols correspond to loss-modulated modelocking, while the solid curves with solid symbols are the result of gain-modulated modelocking. To distinguish between synthesizers, triangular data points correspond to driving with the high-frequency 83712B, while the circular data points correspond to driving with the low-noise 8663A.
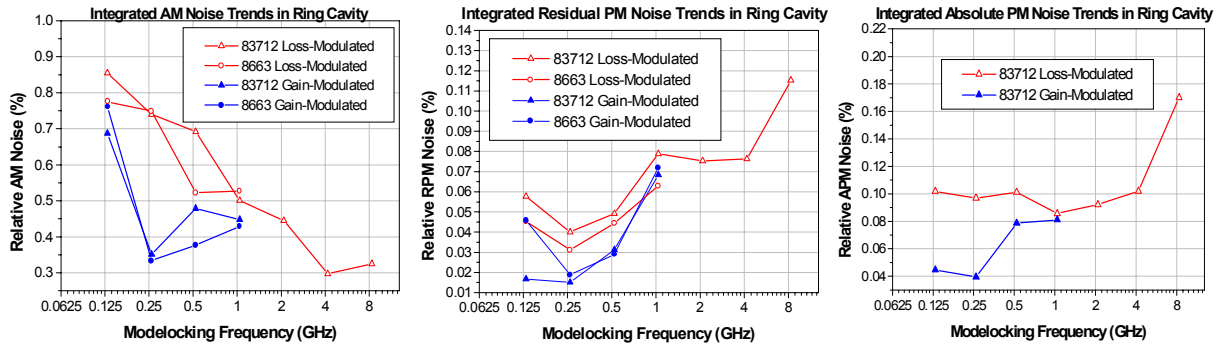
Figure 1.2,1. 3, & 1.4: Left: AM noise, Center: residual PM noise, Right: Absolute PM noise.

Measurements were performed at 2^N harmonics of the fundamental longitudinal mode spacing and were chosen to provide an efficient means for covering approximately two decades of interest in this survey. Changes in noise properties over this operating range do not occur rapidly enough to warrant sampling this frequency range in a linear manner. Errors associated with the measurement process are systematic, and therefore common to all data points.

We begin with an overview of the AM noise results in Figure 1.2. The first salient feature of these curves is that all measured data points reside at a significantly higher RMS noise level than the AM fluctuations of either driving source directly (see Figure 6 for an AM noise curve of the 83712B—the 8663A's curve is comparable). The measured AM noise of the synthesizers is below 0.03% RMS, and the minimal data point in Figure 1.2 surpasses this value by a factor of ten. This suggests that amplitude noise in the synthesizers plays a relatively minor role in shaping the AM noise of the modelocked pulsetrains. This suggestion was confirmed by amplitude-modulating the laser driving signal to produce AM sidebands, and then observing the resulting sidebands in the photodetector signal. The carrier-relative strength (dBc) of the modulation sidebands in the laser signal was seen to have decreased by slightly more than 10 dBc compared to those in the driving signal.

A more interesting feature in Figure 1.2 is the noticeable difference in the AM noise associated with the distinct modelocking techniques (gain versus loss modulation). Loss-modulated modelocking is seen to produce a steady decrease (~0.1% per octave) in AM noise with increasing drive frequency. Gain-modulated modelocking, on the other hand, exhibits a more complicated trend: beginning with slightly lower numbers at 130 MHz, the noise then drops significantly at the next octave, turns slowly upward, and appears to begin merging with the loss-modulated data as 1 GHz is approached. This advantage of gain-modulated modelocking is exhibited in all of the types of noise investigated. Another characteristic common to all noise trends is the upward discontinuity observed in the final octave of modelocking frequency (the transition from 4.15 GHz to 8.3 GHz shows a larger jump than would be expected based on the data's previous trend). Finally, note that the loss-modulated data associated with the lower-noise synthesizer (8663A) falls slightly below that of the 83712B—as will be discussed shortly, the residual phase noise displays the same behavior. The gain-modulated data, however, does not show a noticeable deviation between synthesizers.

Residual PM noise measurements are compiled in Figure 1.3 (RMS units are in percentage of modelocking period). This data reveals a general trend toward increasing noise with modelocking frequency. The lower noise achieved using gain modulation is still present, as is the trend toward convergence between modelocking techniques as the driving frequency approaches 1 GHz. Loss modulation again displays a noticeable offset between synthesizers while gain modulation does not. Finally, the significant discontinuity in the last octave of the loss-modulated data is also observed.

Absolute PM noise measurements are compiled in Figure 1.4. (Since these measurements, by definition, required a reference synthesizer with significantly lower-noise than the one driving the laser, no measurements were made when using the 8663A for modelocking.) These RMS values are slightly higher than the corresponding residual noise values, as expected. Gain and loss modulation again display their characteristic differences, as well as their convergence as 1 GHz is approached. The discontinuity in the last octaves of loss modulation is also observed.

Beginning the discussion with AM noise (Figure 1.2), several comments can be made regarding these results. Spontaneous emission is targeted as the primary contributor to pulsetrain noise in several theoretical papers [23-25]. Success in lowering the amount of spontaneous emission being coupled into extraneous (non-locked) longitudinal modes of the cavity would therefore be expected to have positive consequences. The most general observed trend in Figure 1.2 is the overall decrease in AM noise with increasing modelocking frequency. We believe this to be a consequence of the increase in average pulsetrain power as well as the decrease in pulsewidth that both accompany modelocking at higher frequencies. Over the measured modelocking range, pulsetrain power is observed to change from ~3 mW at 130MHz to ~20 mW at 8.3GHz, while the measured pulsewidth changes from ~220 ps to ~27 ps (for corresponding frequencies). The increase in average power will tend to increase the more fundamental signal-to-noise ratio determined by statistical fluctuations (since smaller statistical noise is known to accompany a larger photon population). In addition, the fact that the ratio of pulsewidth to modelocking period becomes larger (2.9% at 130MHz to 22.4% at 8.3GHz) will tend to reduce the percentage of the period occupied by (noisy) spontaneous emission. (The majority of a well-formed pulse's photon population resides within a relatively narrow optical band.) These effects lower the overall ratio

of average spontaneous emission power to average pulsetrain power, and most likely contribute to the observed decrease in AM noise that occurs with increasing modelocking frequency.

Another aspect to notice in Figure 1.2 is that the AM noise associated with the gain-modulated laser is generally lower than that of the loss-modulated laser. As the pulse passes through the homogeneous gain medium of the diode, photons are primarily stimulated into a relatively narrow optical band, while the random spontaneous emission is temporarily quenched. After the pulse leaves the gain medium, ASE then increases in accordance with the gain recovery time (in the case of loss modulation) or with the pumping rate (in the case of gain modulation). In the loss-modulated case, the ASE emitted between pulses is reasonably constant since the diode is DC biased. Gain modulation, on the other hand, tends to intrinsically decrease the amount of ASE between pulses by effectively shutting off the pumping rate. We attribute the generally better AM noise performance exhibited by gain modulation to the superior manner in which the interpulse ASE is quenched.

A final focus of discussion is the way in which the AM noise of both modelocking methods is seen to converge at higher pulse rates. We believe this to be due to the empirical fact that the DC-component of the drive current used in gain-modulated modelocking must be increased with pulse rate in order to retain a quality modelocked pulsetrain. At lower modelocking rates, the average (DC) level of driving current can be placed well below the threshold current of the laser, resulting in a narrower time window for pulse formation (relative to the modelocking period) as well as an increased window of spontaneous emission quenching over the remainder of the driving cycle. This is in contrast to the DC bias when modelocking with loss modulation, which must always remain above the laser's threshold. As the gain-modulated modelocking rate increases, however, it becomes necessary for optimal performance to increase the DC bias on the diode. This then increases the ASE between pulses, and therefore causes gain modulation to lose its advantage over loss modulation.

Residual phase noise exhibits an opposite trend compared to amplitude noise—appearing to increase with modelocking frequency. We believe this behavior to be associated with a decrease in the energy per pulse as the modelocking frequency increases, which subsequently tends to relax the opposing nonlinear mechanisms that stabilize the positions of each pulse in the time domain. For example, variations in dynamic gain saturation tend to advance the pulse in time, while variations in dynamic index tend to retard the pulse in time [25]. The efficiency of such nonlinear mechanisms decreases with pulse energy. The end result produced by an increase in the pulse repetition rate, then, would be a relaxation of the locking constraints that keep the pulses anchored in the time domain. One can therefore expect a larger variation (noise) in the stabilized variable (time), and hence an increase in the pulse-to-pulse jitter.

An interesting observation in Figures 1.2 and 1.3 is that the loss-modulated laser shows slightly lower amplitude noise and residual jitter when being driven with the synthesizer having the lower phase noise. Residual phase noise, by definition, is a measure of the noise added by the laser, and is theoretically independent of the level of noise in the driving synthesizer. The fact that this trend is observed in the AM noise as well, even though the AM noise of the two driving synthesizers is well below that of the laser, is also interesting. These results suggests two interesting possibilities for the loss-modulated geometry: 1) enhanced AM-PM noise coupling

(compared to gain modulation), and 2) increasing residual phase noise with increasing source phase noise. Loss-modulated modelocking was accomplished through the use of a Mach-Zehnder modulator, which uses the Pockels effect to convert changes in optical index into changes in optical amplitude.. This could provide a possible mechanism for AM-PM coupling, since an instantaneous phase change of the driving signal impresses a new voltage on the modulator, changing the pulse intensity, not it's position. The gain modulated curves, on the other hand, do not show as noticeable an offset between synthesizers, in either AM or residual PM noise. The "residual" nature of phase noise seems more preserved with gain modulation, in accordance with the fairly minor AM-PM coupling mechanisms that are predicted theoretically [25].

The laser's absolute phase noise in Figure 1.4 shows the familiar contrast between gain and loss modulation. The noise of the 83712B synthesizer is known to increase with operating frequency, which explains the general trend in Figure 1.4 (as gain modulation was seen to produce significantly lower residual noise in Figure 1.3, its absolute noise, by definition, more closely matches that of the synthesizer at lower frequencies). However, the deviation of the data over the last two octaves is quite significant. Such a deviation suggests an important change in the laser dynamics at higher modelocking frequencies (specifically between 4 and 8 GHz). This transition is believed to be related to the resonance associated with the relaxation oscillation, which falls within this frequency range.

1.4 Ultralow-Noise Optical Sampling Streams
The low-noise requirements of optical sampling systems become increasingly more difficult to attain as the goals associated with either sampling frequency or bit resolution become more assertive [17]. If performing the sampling with optical pulsetrains, a decrease in pulsewidth must also accompany higher bit rates [6]. We have experimentally investigated the ability of actively-modelocked external-cavity semiconductor diode lasers to meet these requirements, and it is the operating characteristics of our 10 GHz ring laser that will now be presented.

The attributes of our 10 GHz loss-modulated ring laser were investigated using two different geometries. Since earlier experimental results suggested the tendency for noise to increase as the laser is operated with more optical bandwidth [20], lowest-noise operation was initially achieved by incorporating a band-limiting etalon (~7 nm FSR, finesse ~5) into the cavity. Shortest-pulse operation required the removal of the etalon to allow the modelocked bandwidth to broaden considerably. Careful tuning of the modelocking conditions then facilitated the organization of a highly linear chirp [26] which allowed the pulsewidth to be compressed by a factor of ~10 through the use of a dual-grating dispersion compensator. It was seen that the shortest-pulse geometry causes only a slight increase in laser phase noise, but a more appreciable increase in laser amplitude noise.

A restriction on the type of pulsed optical sampling system described here involves the width of the sampling pulses. Taylor has presented an argument for the maximum pulse interaction time allowed when trying to optically sample a signal of bandwidth ν_{sig} while retaining an accuracy of N bits [6]. For a system sampling at the Nyquist frequency, this argument is based on the need to reduce pulse amplitude fluctuations to less than ½ LSB for an input signal covering the full peak-to-peak amplitude range. When amplitude-modulating an optical pulsetrain as it passes through a velocity-matched Mach-Zehnder intensity modulator, it would be appropriate to assume a

gaussian (rather than rectangular) sampling window. Applying this minor revision to Taylor's argument results in the following requirement on the sampling pulsewidth, t_p (FWHM):

$$t_p \leq \frac{2\sqrt{\ln 2}}{\pi \cdot \nu_{sig}} \sqrt{\frac{1}{2^N}} \qquad\qquad (4)$$

This equation, for example, predicts the need for 1.7 ps pulsewidths in order to sample a 5 GHz signal at the Nyquist frequency with 12 bits of resolution.

Figure 1.5 compares the temporal autocorrelations and modelocked optical spectra of the 10 GHz laser when operating both with and without the intracavity etalon. The laser's pulsewidth is seen to decrease from 13 ps to 1.2 ps (after dispersion compensation), while the modelocked spectral width increases from 0.47 nm to 5.1 nm. The time-bandwidth product under both conditions remained the same: ~1.7 times transform-limited. According to equation 4, the narrow-band pulses (13 ps) would allow a resolution of only 2 bits for sampling a 5 GHz signal at the Nyquist frequency, while as many as 12.9 bits of resolution are possible using the 1.2 ps pulses.
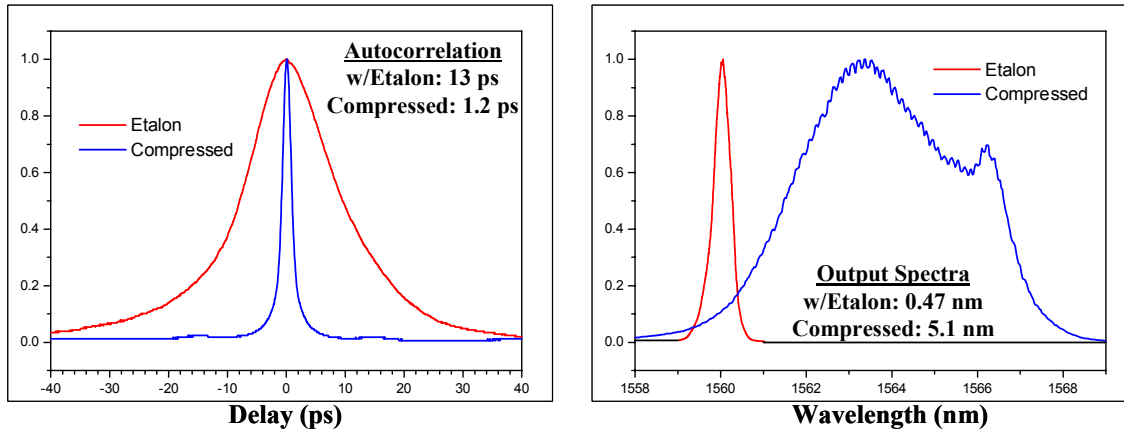
Figure 1.5(a,b): Temporal autocorrelation and optical spectra for laser operation with and without intracavity etalon.

The measured AM noise sidebands of the 10 GHz laser (both in narrow- and wide-band operation) are shown in Figure 1.6, along with the AM noise of the driving synthesizer (83712B). The noise curve for wideband laser operation (without the etalon) possesses a "knee" at approximately 500 kHz offset. This characteristic is due to a well-defined photon correlation time that results from both the cavity round-trip time and cavity Q [25]. This knee becomes washed out (decorrelated) when the etalon is commissioned because a new and unrelated time constant has been added to the resonator. Integration of these noise sidebands over the entire displayed offset range (10 Hz-10 MHz) results in a RMS amplitude fluctuation of 0.27% without the etalon, and 0.12% with the etalon.

In order to estimate the ADC conversion accuracy associated with these results, we identify the most-significant-bit (MSB) with the amplitude of the carrier, and demand that the RMS AM fluctuation correspond to a value less than one-half of the least-significant-bit (LSB). Such an

argument applied over the displayed frequency range suggests a theoretical resolution of 7.5 and 8.7 bits, respectively (independent of the laser sampling rate).

The laser's residual PM noise sidebands are shown in Figure 1.7, along with the residual noise measurement floor. (The noise floor was obtained by referencing the driving signal to itself, and thus represents the amount of noise contributed by the mixer and amplifier used in the measurement system.) The phase noise here is referred to as "residual" due to the fact that the detected laser signal was compared to that of the driving synthesizer, thereby measuring the amount of phase noise added by the laser itself [21]. The knee characteristics are seen to closely resemble those in the AM noise curves (the comparatively well-defined wideband knee becomes washed out during narrowband operation). Integration of the PM noise curves in Figure 1.7 over all displayed frequency offsets gives a RMS jitter of 48 fs for the wideband system and 43 fs for the narrow-band system. Using Walden's result relating equivalent theoretical bit resolution, N, to RMS jitter, τ_j, [17]:

$$N = \log 2 \left(\frac{2}{\sqrt{3}\pi \cdot f_{samp}\tau_j} \right) - 1 \qquad (5)$$

one finds that these levels of phase noise would be sufficient to resolve 8.6 and 8.7 bits, respectively, at a Nyquist sampling rate of 10 GHz.
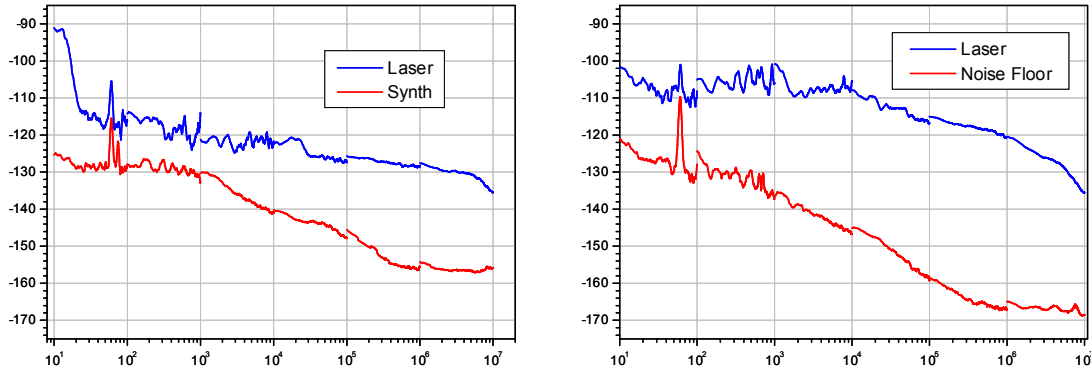
Figure 1.6 & 1.7: Left: Modelocked pulse train AM noise sideband; Right: Residual PM noise sideband for 10 GHz modelocking rates. The measurement noise floor is shown in red.

The complexity with which noise causes and effects are related in this system has motivated a proof-of-principle attempt at reducing laser noise using an empirical strategy—the phase-locked-loop (PLL). Our implementation of this device consisted of a commercial mixer, a commercial voltage-controlled phase shifter, and a home-built amplifier arranged in a negative-feedback geometry designed to promote closer phase tracking of the driving source by the laser (Figure 1.8). Voltage-controlled phase shifters are currently offered in rather limited variety for use with multigigahertz carriers. The commercial unit that had the widest analog response bandwidth was designed for use on a 2 GHz carrier frequency, which required the laser to be modelocked at the 31st harmonic.
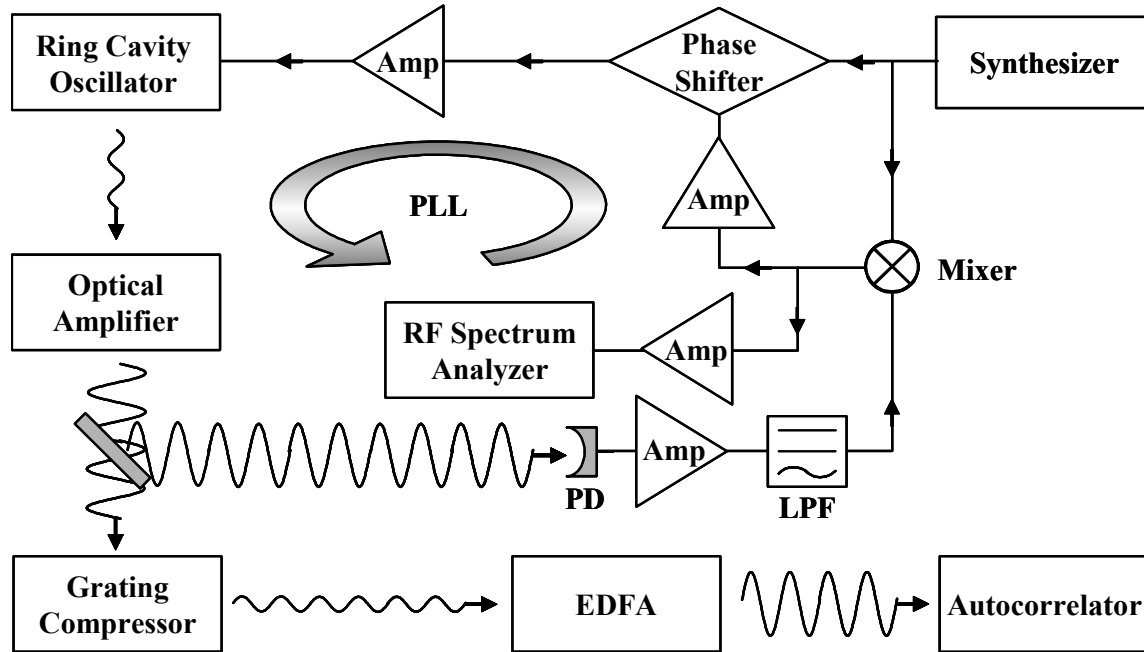
Figure 1.8: Schematic of the phase lock loop to reduce timing close to the carrier.

Results of the 2GHz locking test are shown in Figure 1.9. The three curves represent the laser's residual PM noise under normal operation, the noise of the laser being reduced through PLL action, and the measurement system noise floor. By phase-locking the laser to the driving signal, residual PM noise was reduced by almost 30 dB within the response band of the phase shifter. Unfortunately due to the shape of the laser's phase noise spectra, the bulk of the noise energy resides in the offset frequencies surrounding the knee ($\sim10^5$-10^7 Hz) which is beyond the response bandwidth of the fastest phase shifters currently available. To quantify the impact of the PLL, however, one may integrate the noise sidebands within the PLL response band (out to ~100 kHz—the dark vertical line in Figure 1.9) to learn that this in-band RMS noise has been reduced by 91% from 88 fs to 8 fs.

It should be noted that the point of this demonstration is to show that the residual phase noise can be substantially reduced (~30 dB) by pure electronic means, as compared to conventional methods using electro-mechanical means, e.g., piezoelectric transducers, over the bandwidth of the phase locked loop. In addition, the result points to the potential of employing voltage controlled phase shifters at 10 GHz, with correspondingly larger response bandwidths, such that the bandwidth of the phase locked loop is commensurate with the knee or roll-off

Figure 1.9: Experimental result showing the phase noise reduction of the phase locked loop

13

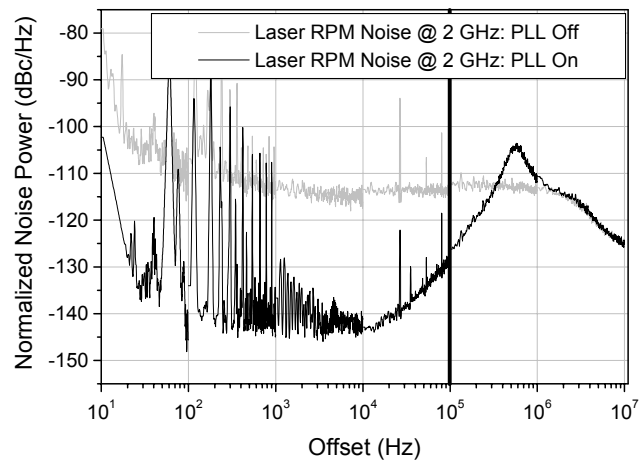frequency of the RPM noise spectra. This would result in a RPM noise spectra that has a phase noise floor of −140 dBc/Hz extending from 100 Hz to 5 GHz. Given access to phase-shifting components that are capable of operating on higher carrier frequencies with greater response bandwidths, the ability to reduce pulsetrain phase noise below the previously reported 43 fs should be possible.

1.5 Noise Measurements at Large Offset Frequency

Measured carrier noise spectral densities have traditionally been confined to relatively narrow bands of offset frequency, the limitations being determined primarily by restrictions in the measurement electronics. In an ideal attempt to measure RMS noise based on a spectral scan, however, one would like to characterize a continuous-wave source over an infinitely long time period, with infinitely fine temporal resolution, so as to capture both the lowest- and highest-frequency components in the noise. Practicality requires a compromise on these ideals.

The lower cutoff of offset frequency (where to begin the integration) can be chosen based on the amount of time one is willing to spend making the noise measurement. This time interval represents the lowest frequency over which any changes in signal can be detected. The upper cutoff is a different matter. A periodic process such as an optical pulsetrain is composed of several Fourier components, each of which is readily marked in the frequency domain. Noise sidebands associated with the fundamental carrier (or any carrier harmonic, for that matter) can only be distinguished out to the Nyquist offset frequency. Beyond this offset, the noise energy of adjacent harmonics begins to surpass that of the harmonic in question. For this reason, the Nyquist frequency serves as a distinctive barrier between any particular harmonic and it's nearest neighbor. Noise fluctuations beyond this frequency offset can no longer be ascribed to the particular carrier under scrutiny. It is for these reasons that we have attempted the first measurements of noise spectral density out to Nyquist frequency offsets for our 10 GHz laser system.

Figure 1.10 displays the noise sidebands of the (broadband) 10 GHz ring laser measured out to the Nyquist offset. Three separate amplifiers were used to boost the noise power after carrier mixing in order to cover the offset range of interest. The plotted curves represent the laser's residual PM noise (dotted), an "effective" noise floor that will be explained shortly (gray), and the ultimate noise floor of our measurement system (black). The spikes occurring over the last three decades are associated with longitudinal supermode beating.

It should be stressed again that supermode noise has been ignored in the integration, owing to the unresolved issue as to whether these components primarily effect AM or PM noise.   Again, it should be noted that the suppression of supermode noise to −140 dBc/Hz has recently been demonstrated, which negates the need of their inclusion in the integration of noise (see Section 3).

Integration of the laser's noise curve over all displayed frequencies results in an upper bound on the RMS jitter of 121 fs. Such a value of pulsetrain jitter would theoretically provide 7.2 bits of resolution.
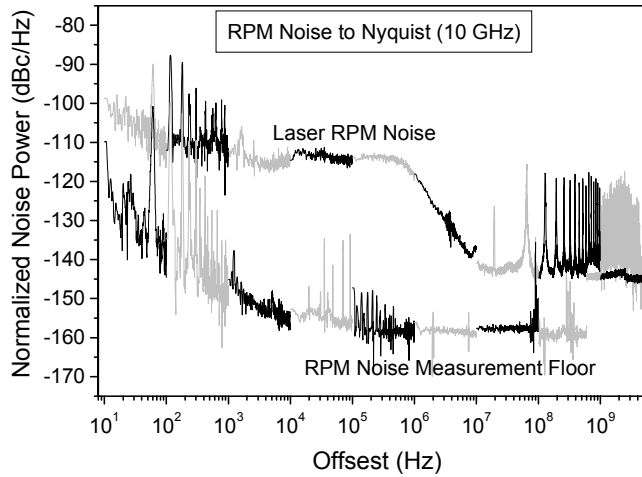
Figure 1.10: Residual phase noise measured to Nyquist offsets for 10 GHz modelocked pulsetrain.

Beyond offset frequencies of 10 MHz, the measured noise displays a white characteristic. This observation invites a new kind of speculation—does this noise truly represent the laser's behavior, or is it a result of limitations in measurement? The fact that the spikes due to longitudinal mode beating possess peak values in excess of 20 dB above the white noise floor lends a certain amount of validity to their numbers, but the level of the white noise floor itself must be scrutinized. The average power in the 10 GHz fundamental of the signal immediately after photodetection was measured to be roughly -20 dBm. This resides ~153 dB above thermal noise at room temperature. If one assumes that no significant noise figures exist within the detection/measurement system, then this would represent the maximum dynamic range that can be achieved in the phase noise measurement (153 dBc). The measured white noise floor in the phase noise of the laser resides at -145 dBc, only 8 dB above this thermal limit (an amount that could easily be attributed to amplifier noise figures or conversion loss in the mixer). In an effort to confirm this empirically, a measurement was arranged to simulate the expected "experimental" noise floor. Two identical synthesizer signals at ~0 dBm are normally used to test the residual noise measurement floor (black curve in Figure 10). If one of these signals is first attenuated to the level of the photodetector output (-20 dBm) and then sent through the same RF amplifier that is used to experimentally boost the detector signal, an "effective" residual noise measurement floor that is more representative of the experimental conditions will be measured. The result of such a measurement is a greatly compromised "effective" noise floor (gray curve). In fact, the effective white noise floor in Figure 10 resides only 5 dB below the measured laser noise. This implies a strong possibility that the displayed laser noise floor is due to measurement limitations rather than the laser itself, and tends to bring the validity of the total RMS jitter quoted earlier into question. It is for this reason that the measured value of 121 fs is referred to as an upper bound

1.6 Conclusion for Section 1
We have presented an external-cavity, actively-modelocked semiconductor diode ring laser capable of extremely high stability. Gain modulation was found to produce modelocked pulsetrains with better noise characteristics at lower driving frequencies due to a more efficient quenching of intracavity spontaneous emission. Modelocked pulsetrains at 10 GHz exhibited pulsewidths as low as 1.2 ps, amplitude noise as low as 0.12% RMS (10 Hz-10 MHz), and residual phase noise jitter as low as 43 fs RMS (10 Hz-10 MHz). The stability of these sampling streams would provide a resolution of 8.6 bits in a photonic analog-to-digital converter sampling at 10 GHz. A proof-of-principle reduction of in-band RMS phase noise by as much as 91% was accomplished through implementation of a home-built phase-locked-loop. Finally, the

measurement of high-frequency laser phase-noise out to the Nyquist offset has been accomplished for the first time at a 10 GHz carrier frequency, resulting in an upper limit of RMS jitter of 121 fs (10 Hz-5 GHz).

SECTION 2:

We report what are to our knowledge the first AM and PM noise measurements out to Nyquist frequency offsets for an external cavity semiconductor laser hybridly modelocked at 10 GHz. The differing noise properties of a fundamentally modelocked and a harmonically modelocked cavity (both producing 10 GHz pulsetrains) are compared.

2.1 Introduction

Modelocked semiconductor and fiber lasers have been shown to operate with very low noise levels making them suitable as sources of sampling pulses for applications in analog-to-digital converter (ADC) technologies [27-30]. In spite of the need for long cavities in fiber lasers, obtaining multigigahertz sampling rates has been possible by harmonic modelocking at high integer multiples of the relatively low fundamental cavity frequencies. Semiconductor lasers, on the other hand, have the capability of operating in both regimes (cavities can be either long or short). For harmonically modelocked lasers, noise spurs will arise at harmonics of the cavity frequency, while fundamental modelocking has the ability to eliminate these spurs.

At multigigahertz sampling rates, every doubling in the sampling frequency causes the resolution to fall by ~1 bit due to phase modulation (PM) noise (timing jitter) in the sampler [31]. Accurate evaluation of pulsetrain noise then becomes an important issue. Commonly, reported measurements of PM noise extend out to limited offset frequencies (several tens of megahertz or lower) [27-30]. To consider the noise characterization complete, however, sideband measurements should extend to the highest offset frequencies possible (i.e. the Nyquist frequency). For harmonically modelocked lasers, this offset range will include noise spurs arising from harmonic beating mechanisms.

In this report, we show measurements of AM and residual PM noise out to the Nyquist offset frequency (5 GHz) of a hybridly modelocked external cavity semiconductor laser for fundamental cavity frequency modelocking as well as harmonic modelocking.

2.2 Experiment and Results:

The 10 GHz laser cavity is shown in Figure 2.1. 1550 nm light from the anti-reflection (AR)
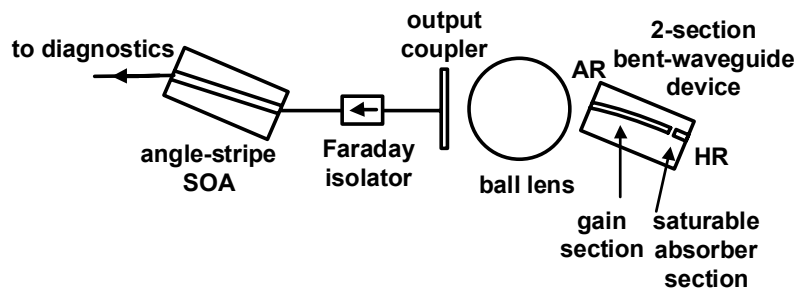

Fig. 2.1 Cavity geometry for the 10 GHz modelocked laser

coated facet of a 2-section bent waveguide device was collected and collimated by a 5 mm diameter ball lens. A 90% reflecting output coupler (OC) and the high-reflector (HR) facet of the bent waveguide device formed the two ends of the laser cavity. The gain section of the 1.5 mm device was DC biased at 60 mA and the 50 μm long saturable absorber (SA) section was reverse biased at –5 V while 10 GHz radio frequency (RF) modulation was applied to the SA section. When the SA section was unbiased, the lasing threshold was measured to be 30 mA of gain section current. The average power from the modelocked laser was 1.3 mW and it was amplified to 11 mW with a 2.3 mm long angle-stripe semiconductor optical amplifier (SOA). The SOA output was detected with a 15 GHz photodetector for AM and residual PM noise measurements.

An Anaren 7312B mixer was used as both the AM and the PM detector. To measure AM noise, the amplified photodetector signal was split with a 3 dB power splitter and sent in phase to the two ports of the mixer [32]. This technique translates the carrier noise sidebands to baseband and cancels the laser PM noise at the mixer output while the mixer is at maximum sensitivity to AM.

Residual PM noise was measured by the phase detector method [28]. The amplified photodetector signal was mixed in quadrature (90° phase difference) with a split portion of the signal from the RF synthesizer that modulated the laser for modelocking. The RF synthesizer PM noise was taken out, leaving the noise due directly to the laser. Due to the quadrature condition the mixer was at maximum sensitivity to phase fluctuations.

Figures 2.2(a) and 2.2(b) show the AM and residual PM noise, respectively, measured with the techniques described above when the fundamental cavity frequency was adjusted to be 10 GHz. A knee occurred at an offset frequency of about 55 MHz. Integration of the curves (10 Hz-5 GHz) gave 0.11% RMS pulse intensity fluctuations and 670 fsec RMS timing jitter. The integration was carried out assuming the roll-off of the curve after the knee (~25 dB/decade) extends out to the Nyquist frequency offset, as predicted by theory [33,34].

Figures 2.3(a) and 2.3(b) show the AM and residual PM noise, respectively, measured when the
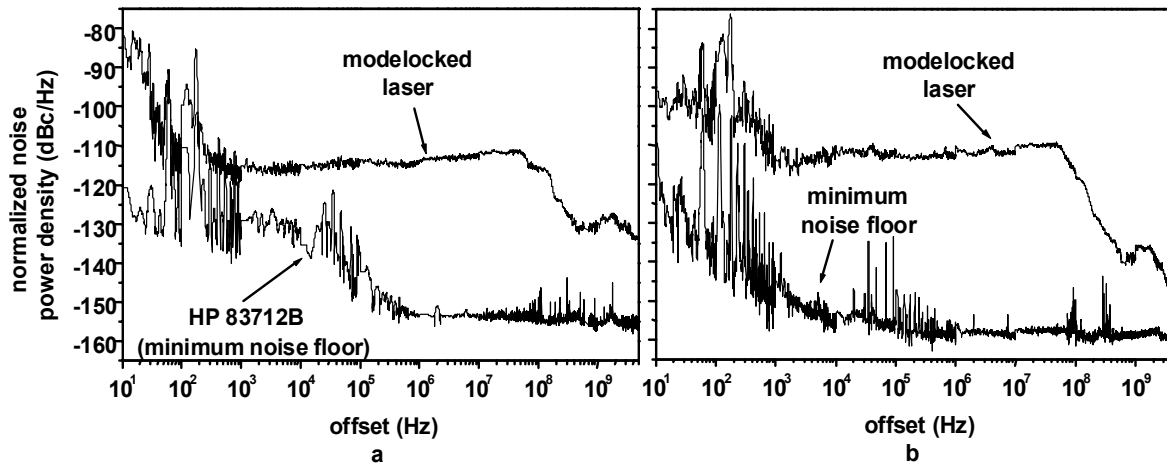

Fig. 2.2 Noise sidebands for modelocking at 10 GHz with 10 GHz cavity fundamental frequency and noise floors

(a) AM noise (b) Residual PM noise

10 GHz modelocking rate corresponded to the 68th harmonic of the cavity fundamental (147 MHz). Compared with Figures 2.2(a) and 2.2(b), the knee moved in to about 600 kHz and spurs

appeared at offset frequencies of harmonics of the cavity fundamental. Integration of the curves gave 0.05% RMS pulse intensity fluctuations and 240 fsec RMS timing jitter, again assuming the 25 dB/decade roll-off after the knee. The peak power density of the spurs were at −100dBc/Hz for the AM noise and −95dBc/Hz for the residual PM noise.
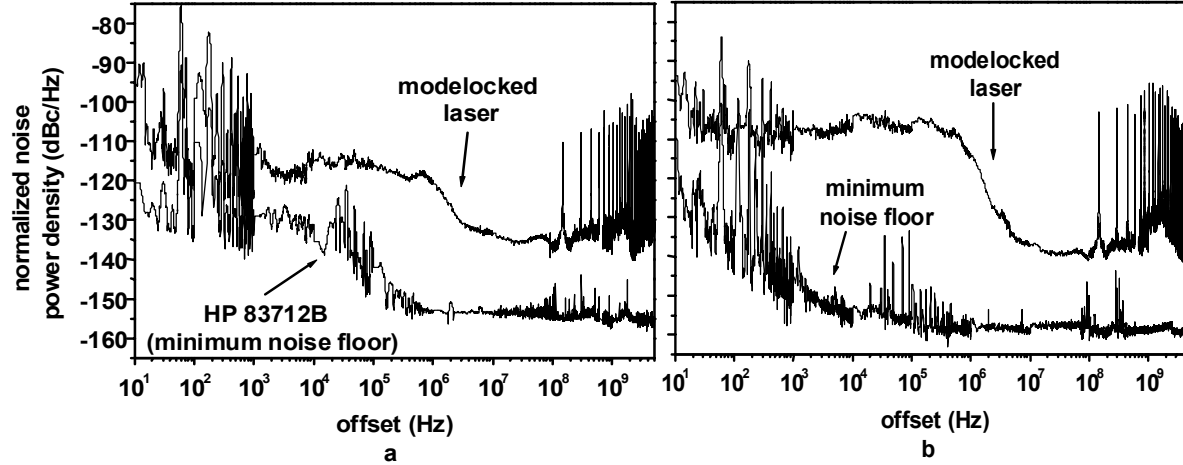

Fig. 2. 3 Noise sidebands for harmonic modelocking at 10 GHz with 147 MHz cavity fundamental frequency and noise floors

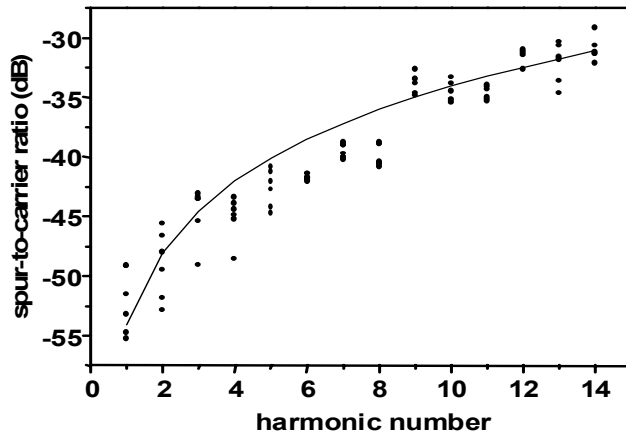(a) AM noise (b) Residual PM noise

Fig. 2.4 Spur-to-carrier ratios of harmonics of 1.9 GHz modelocked laser with 147 MHz fundamental cavity frequency
• Measured data; _____ Quadratic fit to data

PM noise can also be extracted by comparing the noise sidebands at harmonics of the fundamental modelocking frequency, as suggested by Von der Linde [35]. Sideband power normalized to its carrier depends quadratically on harmonic number when AM noise is much less than PM noise. To determine whether the cavity harmonic spurs represent AM or PM noise, the peak values of the spurs around the harmonics of the modelocking frequency were measured. Due to the bandwidth limitations of the 40 GHz photodetector and the 50 GHz RF spectrum analyzer used in these measurements, to be able to observe high harmonics of the modelocking frequency, the laser was harmonically modelocked at 1.9 GHz with 147 MHz fundamental cavity frequency. The peak powers of the spurs around the harmonics of 1.9 GHz up to the 14th harmonic (26.8 GHz) were then measured.

Figure 2.4 shows a scatter plot of the spur-to-carrier ratio as a function of harmonic number. The data points at each cavity harmonic represent the spur-to-carrier ratio of that harmonic's six closest spurs. The solid line in figure 4 is the quadratic fit to the data (in dB units). The quadratic dependence of the spur-to-carrier ratio on harmonic number suggests that the noise in the spurs is predominantly PM noise. The spurs have commonly been considered to represent AM noise and disregarded in timing jitter analyses. However, the present result points to the importance of their consideration in PM noise characterizations of harmonically modelocked lasers.

2.2 Conclusion for Section 2

For the first time to our knowledge, the AM and residual PM noise for a 10 GHz modelocked laser has been measured out to Nyquist offsets. In addition, the noise spurs in our harmonically modelocked laser system were found to consist primarily of PM noise, in contrast to conventional assumptions.

3.1 Introduction

One of today's most popular optical gain media for telecommunications, the Erbium-doped fiber amplifier (EDFA), possesses an intrinsically low gain per unit length, therefore forcing fundamental cavity frequencies of closed optical resonator systems to remain in the 10 MHz regime. Their wideband spectral characteristics allow the capacity for optical frequency tuning over a wide range, but also necessitate the need for harmonic modelocking at extremely high orders to achieve the bit rates typically desired for most current applications. Semiconductor optical amplifiers (SOAs) are known to possess the attractive property of high gain per unit length, but have been somewhat overlooked due to the widely-held belief that their application in telecommunication arenas will be limited due to their noise properties.

In this report, we submit further evidence supporting the notion that such devices are, in fact, capable of the extremely low-noise properties needed for applications at high bit rates. Experimental results are presented for an external-cavity semiconductor diode laser geometry operating at 10 GHz which has achieved both the lowest modelocked pulsetrain noise to date for such systems, as well as a thorough suppression of the supermode noise (intrinsic to all harmonically-modelocked lasers) by using an intracavity etalon [36]. More importantly, a novel technique of sideband noise measurement out to Nyquist offset frequencies (5 GHz) reveals that even with supermode noise suppressed below the laser noise floor, the noise spectrum still retains the low-offset knee characteristic of long-cavity lasers. The two decades of offset frequency surrounding the knee in the noise sideband are typically responsible for as much as 95% of the RMS pulsetrain fluctuation, therefore it is desirable to keep the knee as close to the carrier as possible to minimize the noise integral. We compare these results to similar systems with shorter cavities (namely a SOA laser fundamentally-modelocked at 10 GHz) in which the shorter cavity correlation time pushes the knee out to much larger offset frequencies [37]. This result, therefore, implies an intrinsic advantage to using harmonically-modelocked systems when the supermode noise is sufficiently suppressed.

3.2 Experimental Results

The experimental geometry is illustrated in Figure 3.1. Since polarization properties are critical for best noise performance, no mirrors are used in the ring cavity. The free-space section contains extensive
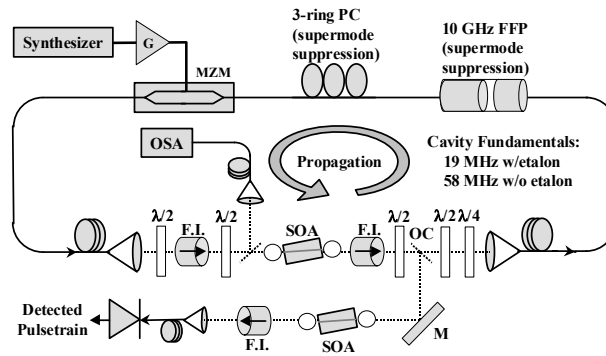

Fig. 3.1. Experimental Layout. (SOA: semiconductor optical amplifier, F.I.: Faraday isolator, OC: output coupler, MZM: Mach- Zehnder modulator, PC: polarization controller, FFP: fiber Fabry-Perot.

isolation and polarization-controlling optics surrounding an InGaAsP SOA. In order to operate the laser with suppressed supermodes, a high-finesse (~180) 10 GHz fiber-Fabry-Perot (FFP) filter and 3-ring polarization controller (PC) are inserted in the cavity prior to injection into the PM-fiber-pigtailed Mach-Zehnder modulator (MZM). The fundamental cavity frequency without the intracavity FFP and PC is 58 MHz, and the incorporation of the etalon components reduces this to 18 MHz. Cavity output coupling is achieved through the use of an uncoated 3 μm pellicle beamsplitter operating on P-type polarization for minimum reflectivity (highest cavity Q). The pulsetrain then undergoes amplification with a single pass through a second SOA. Additional isolation follows the amplifier diode before the free-space pulsetrain is launched into a single-mode fiber-pigtailed detector (14 GHz bandwidth). Noise measurements of both amplitude and residual phase are then performed using a recently-reported wideband variation [37] of a commonly-used mixing-to-baseband technique [38].

Figure 2(a) shows the results of wideband noise measurements (both AM and residual PM) for the extended-cavity modelocked laser, and Figure 2(b) shows similar measurements with a fundamentally-modelocked SOA system reported recently (for comparison) [37]. The lowest noise properties to date (Figure 2(a)) were achieved using a 1.0mm InGaAsP SOA as the optical
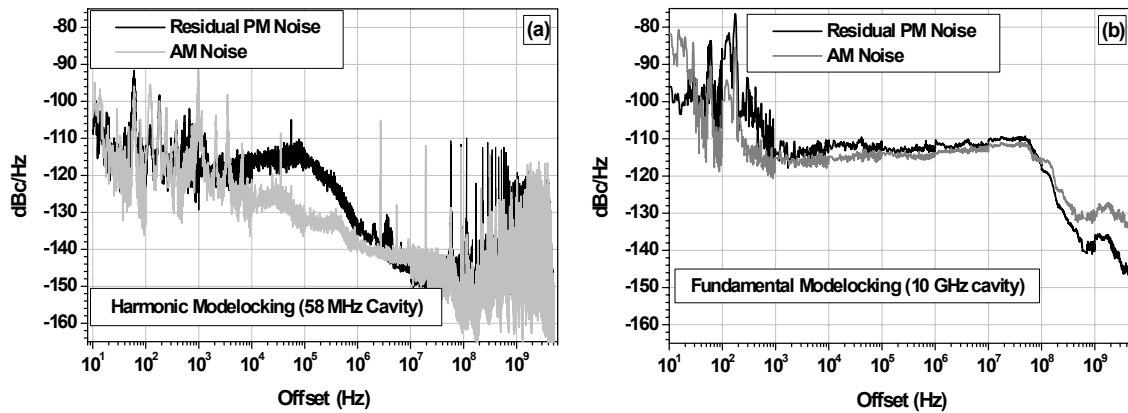

Fig. 3.2: Modelocked laser noise sidebands for harmonic modelocking (a) and fundamental modelocking (b) at 10 GHz.

gain medium. The important features include the position of the knee in the harmonically-modelocked PM noise curve at roughly 80kHz offset (compared to 55MHz for the fundamentally-modelocked cavity), as well as the distinct observation of supermode noise throughout the last three decades (which is absent in thefundamentally-modelocked case). It should be noted that the supermode noise, thought to be solely an amplitude noise phenomenon, is observed prominently in the phase noise spectrum as well. This is a result of the strong AM-PM coupling characteristics of semiconductor lasers. Integrating the curves in figure 2a out to 10 MHz (a standard offset frequency) gives RMS noise values of 18 fs residual PM noise and 0.05% AM noise (compared to 193.5 fs and 0.97% for the fundamentally-modelocked case). Integration of these curves out to the Nyquist frequency of 5 GHz (excluding the supermode noise spikes) results in RMS fluctuations in phase and amplitude of 94 fs and 0.74%, respectively (compare to 664 fs and 4.58% in figure 2b). We believe the results for the harmonically-modelocked system represent the lowest noise characteristics measured to date for an actively-modelocked, external-cavity semiconductor diode laser.

It is obvious that the supermodes will significantly contribute to the noise integrals in figure 2a. To alleviate this problem, a 10 GHz high-finesse intracavity etalon was inserted into the ring cavity. The fiberized etalon is a significantly polarization-sensitive device, the sensitivity of which increases with finesse. For this reason, additional polarization control was used, both before entry into the FFP (l/2 and l/4 plates) as well as following the FFP (3-ring PC). To overcome a significant amount of additional loss, a longer (2.3mm) SOA was used as the gain medium.

The etalon encourages strong coupling among only a single set of longitudinal modes spaced by 10 GHz (as opposed to multiple sets of supermodes). The etalon's high finesse allows only ~3 longitudinal modes through it's transfer function, which necessitates extremely accurate tuning of the modelocking frequency relative to the fundamental frequency of the etalon. Provisions for tuning the optical path length of the cavity were used to facilitate the alignment of a single set of longitudinal modes with the etalon's transfer function. This alignment showed significant improvements in pulsetrain noise, but was seen to be significantly less critical than matching the modelocking frequency to the etalon's FSR [39].
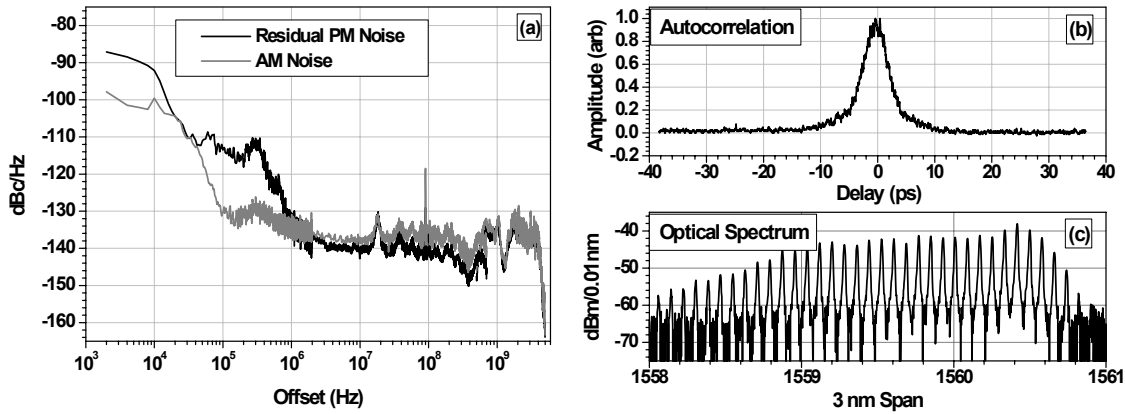

Fig. 3. 3. Modelocked laser noise sidebands showing suppressed supermodes using fiber-Fabry-Perot etalon (a), modelocked autocorrelation trace (b), and high-resolution modelocked optical spectrum (c).

The results of efficient supermode coupling are illustrated in Figure 3, which shows AM and residual PM noise sideband measurements out to the Nyquist frequency (3a), the modelocked pulse autocorrelation function (3b), and the modelocked spectrum (3c). As seen in Figure 3a, the knee position remains at low offset ~300kHz, while the suppression of supermode noise is almost total. The first three supermodes in decade 7 are not completely attenuated below the noise floor as they reside within the passband of the etalon. Figure 3b illustrates the pulsewidth autocorrelation, showing pulsewidths of 3.5 ps, and figure 3c illustrates the locked optical modes at a spacing of 10 GHz (optical spectrum analyzer at 0.01nm resolution).

3.3. Conclusion for Section 3
Using active harmonic modelocking at 10 GHz with extensive polarization control in a mirrorless ring geometry, we have achieved what are, to our knowledge, the lowest noise characteristics yet reported for an actively-modelocked external-cavity semiconductor diode laser. Residual RMS jitter as low as 18 fs (10Hz–10MHz) and 94 fs (10Hz-5GHz) has been

measured, as well as RMS amplitude noise as low as 0.05% (10Hz-10MHz) and 0.74% (10Hz-5GHz). In addition, using a high-finesse fiber-fabry-perot intracavity etalon, we have demonstrated nearly complete supermode suppression out to the Nyquist limit, while favorably retaining a low-offset noise knee.

4.1 Introduction

Modelocked semiconductor lasers offer themselves as low timing jitter clocks at multi-GHz sampling rates [40], useful for applications in analog-to-digital conversion and optical sampling. The pulse-to-pulse timing jitter in the pulsetrain is proportional to the square root of the integral of the residual phase noise power spectral density [41]. Comparison of residual phase noise measurements of fundamentally and harmonically modelocked lasers at a 10 GHz modelocking frequency reveals a distinctive knee with a steep roll-off that moves in to lower offset frequencies with increasing cavity length [42]. Since the two decades of offset frequencies around the knee constitute about 90% of the area under the phase noise curve, the position of the knee primarily determines the magnitude of the pulse-to-pulse timing jitter. Thus the lower the knee offset frequency, the smaller the pulse-to-pulse timing jitter. These statements ignore the presence of the supermode noise in harmonically modelocked lasers that manifests itself as noise power spurs at harmonics of the laser fundamental cavity frequency. The exclusion of the supermode noise in calculating timing jitter assumes the suppression of the noise tones at the cavity harmonics. It has recently been demonstrated that supermode noise suppression to levels below –140 dBc/Hz can be achieved without changing the location of the phase noise knee by using a high-finesse intracavity etalon [43]. For continuously operating lasers, it is well known that the noise properties are directly related to the linewidth of the lasing mode [44]. In this Letter, we present measurement results on the residual phase noise knee position and longitudinal mode linewidth as a function of laser cavity frequency for a hybridly modelocked external linear cavity semiconductor laser. We show that the knee position and the average linewidth of the individual modelocked longitudinal modes are directly correlated with each other. This result shows that the average linewidth of the individual modelocked longitudinal modes can be measured by using residual noise measurement techniques, or conversely, the limits of RMS pulse-to-pulse timing jitter is determined by the linewidth of the modelocked longitudinal modes.

4.2 Experiment and Results

Figure 4.1 illustrates the experimental setup. The oscillator is a 1.5 mm long, 2-section bent waveguide device with a 50 μm long saturable absorber (SA) section, operating at 1550 nm. The facet on the SA section side is the high-reflector (HR) facet and the other facet has an anti-reflection (AR) coating. An external cavity was formed by the HR facet and a 90 % reflectivity output coupler placed on the AR coated facet side. A ball lens with a diameter of 5 mm collimated the light onto the output coupler. The gain section of the device was biased at 65 mA. Passive modelocking at the cavity fundamental was obtained by applying a 5-6 V reverse voltage bias on the SA section. Hybrid modelocking was achieved by superposing a radio frequency (RF) signal on the SA section reverse bias. The laser cavity length could be adjusted to correspond to fundamental cavity frequencies up to 10 GHz by translating the output coupler. A 2.3 mm long angle-striped SOA amplified the 1 mW of output power from the modelocked laser to 11 mW. Faraday isolators of >40 dB isolation were used between the laser oscillator and the SOA as well as after the SOA to reduce the light traveling in the backward direction. Residual phase noise was measured using a double-balanced mixer (Anaren 73128) as a phase detector[2]. The longitudinal mode linewidth was measured by the heterodyne beating [45] of the

modelocked laser signal with a tunable semiconductor laser (Santec TSL-210) having a -3 dB linewidth of 500 kHz. The signals from the modelocked laser and the tunable laser were
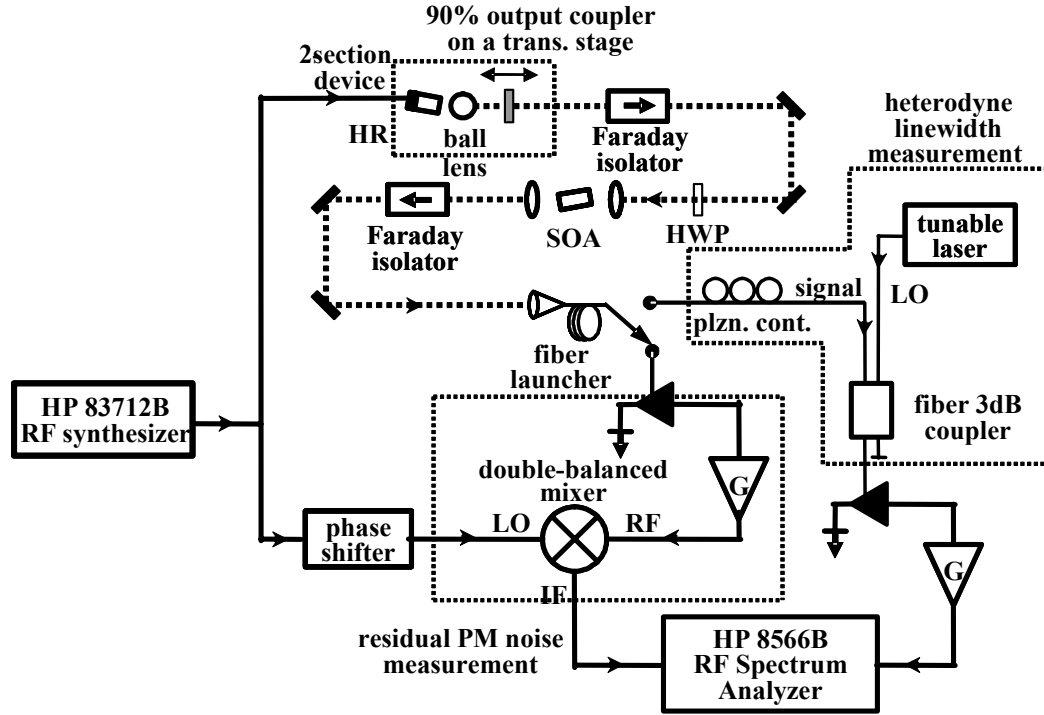

Figure 4.1: Experimental layout (HR: high reflector, SOA: semiconductor optical amplifier, HWP: half-wave plate, G: amplifier).

polarization matched using a 3-ring polarization controller to maximize the beat signal power and combined in a fiber 3 dB coupler. The beat tones representing the longitudinal mode lineshapes had at least 30 dB signal-to-noise ratios as displayed on the RF spectrum analyzer. The -3 dB longitudinal mode linewidths were measured from these beat tones.

Figures 4.2(a) and 4.2(b) show the residual phase noise curves measured for fundamental and harmonic (at the 68th cavity harmonic) modelocking at 10 GHz, respectively. We extended the previous measurements in the 10 Hz-10 MHz offset range [40] out to 5 GHz in order to accurately measure the residual phase noise spectra for modelocking at high repetition rates [42]. In figures 2a and 2b the knees where the 25 dB/decade roll-off starts are at 55 MHz and 600 kHz for the fundamentally and the harmonically modelocked cases, respectively. The RMS
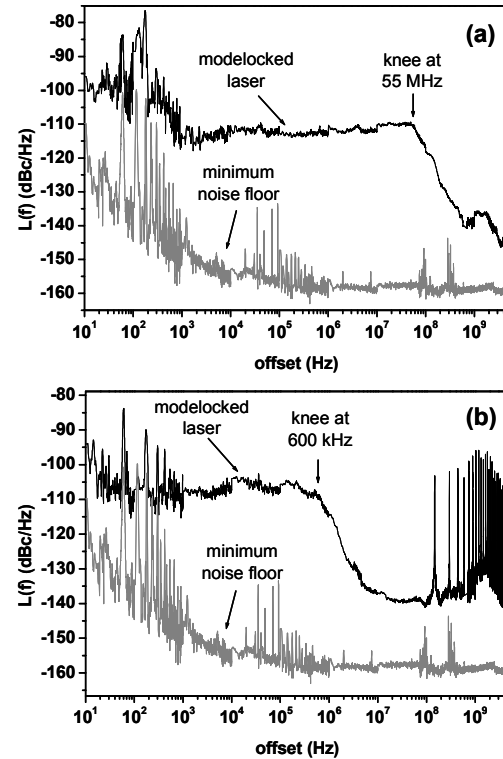

Figure 4.2: Residual phase noise sidebands for modelocking at 10 GHz at the fundamental cavity frequency (a) and at the 68th harmonic (150MHz cavity) (b).

25

pulse-to-pulse timing jitter was calculated by integrating the residual phase noise power density using the expression [46]

$$\Delta t = \frac{1}{2\pi f_{ML}} \left(2 \int_{f_{low}}^{f_{high}} L(f) \; df \right)^{1/2}$$

where f_{ML} is the modelocking frequency, f_{low} and f_{high} are the lower and upper limits of the offset frequency range to be integrated, respectively, and L(f) is the single sideband residual phase noise power normalized to the carrier power (in 1 Hz). Integration of the phase noise curves in figures 4.2(a) and 4.2(b) gave 670 fs and 240 fs RMS pulse-to-pulse timing jitter, respectively. The integration was carried out assuming that the roll-off of the curve after the knee (25 dB/decade) extended out to the Nyquist frequency offset, as predicted by theory [47,48]. The noise tones at the harmonics of the cavity frequency were not included in the integration for the case of harmonic modelocking since their near complete suppression has been demonstrated [43]. It should be stressed that the key point of this report is to identify the relationship between the residual phase noise knee position and longitudinal mode linewidth as well as their influence on pulse-to-pulse timing jitter.

Figure 4.3(a) shows the results of longitudinal mode linewidth measurements of the hybridly modelocked laser at different cavity lengths. The laser was modelocked at the cavity fundamental when the cavity length corresponded to 6.7 GHz and 8 GHz. At other cavity lengths, it was modelocked at 10 GHz. The longitudinal mode linewidths (filled squares) were measured at the Stokes, the central, and the anti-Stokes regions of the optical spectrum. At each cavity frequency setting, 3 linewidth measurements were made from each spectral region considered, for a total of 9 data points. The average linewidths were found to be similar in the Stokes and central regions of the modelocked optical spectrum with the anti-Stokes region having the largest linewidths at all cavity lengths, thus the spread in the data. In Figure 4.3(a), the average longitudinal mode linewidth (open squares), which is approximately linear with cavity frequency, the standard deviation around the average, and the linear fit to the average longitudinal mode linewidth (dashed line) are also displayed. Figure 4.3(b) shows the knee position (filled squares), which is also approximately linear with cavity frequency, and the average linewidth (open squares) as well as their linear fits. The two linear fits match closely, implying a direct relationship between the residual phase noise knee position and the average longitudinal mode linewidth of the modelocked laser.
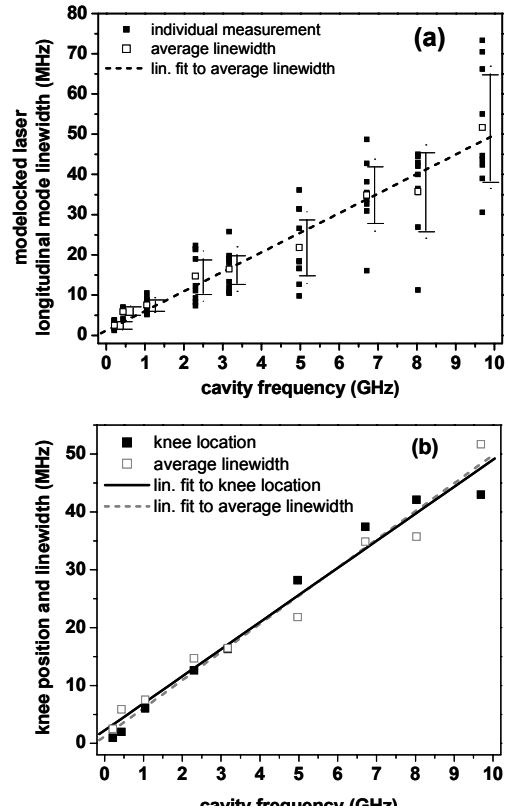

Figure 4.3: Hybridly modelocked laser longitudinal mode linewidth versus cavity frequency (a); average longitudinal mode linewidth and residual phase noise knee position versus cavity frequency and their linear fits (b).

It has been demonstrated that the coherence time of a modelocked pulsetrain is given by the inverse longitudinal mode linewidth [49]. Considering the temporal separation between adjacent pulses, the average linewidth measurement results in Figure 4.3 imply that adjacent pulses in the modelocked pulsetrain are highly coherent at each cavity frequency. This coherence also means that the noise fluctuations in adjacent pulses are highly correlated, making the relative noise fluctuations between these pulses small. However, for pulses separated by increasing time intervals, the inter-pulse coherence as well as the noise correlation gets weaker until there is no coherence and noise correlation left for pulses separated by more than the coherence time. This corresponds, in the residual phase noise, to an increase in the noise power density from high offset frequencies (pulses separated by short time intervals) to low offset frequencies (pulses separated by long time intervals). Eventually the residual phase noise density becomes white for offsets smaller than the knee position (pulses separated by time intervals longer than the coherence time of the pulsetrain). In this way, the coherence time, or equivalently, the average longitudinal mode linewidth of the modelocked pulsetrain determines the residual phase noise knee position.

The quality-factor (Q-factor) of the laser cavity is defined as the ratio of the free spectral range (FSR) to the -3 dB bandwidth of a single transmission peak of the cavity. It is reasonable to expect that as the cavity length is changed by translating the output coupler, the laser cavity Q-factor does not change significantly. As a result, as the FSR of the cavity is changed, the linewidth changes proportionally, resulting in the linear dependence of the average longitudinal mode linewidth on cavity frequency, as shown in Figure 4.3. The proportionality between the phase noise knee offset frequency and the inverse cavity roundtrip time has been pointed out by Hjelme and Mickelson [47], however, to our knowledge, the fundamental relationship between the residual phase noise spectrum and the longitudinal mode linewidth has not been identified.

4.3 Conclusion for Section 4
In summary, we have shown that the knee position in the residual phase noise of our hybridly modelocked external linear cavity semiconductor laser increases linearly with cavity frequency and is determined by the average longitudinal mode linewidth. This suggests that, to attain ultra-low jitter modelocked lasers, methods for reducing the longitudinal mode linewidth are required.

CONCLUSION

We have shown that semiconductor modelocked diode lasers can generate optical pulse trains will ultralow amplitude and timing noise. These pulse trains can be used as optical samplers in applications in photonic analog to digital converters and ultrahigh bit error rate test systems.

RECOMMENDATION

In order to push the performance of ultralow noise optical clocks based on semiconductor gain media, one should 1) employ long optical cavities, 2) perform harmonic modelocking, and 3) use supermode suppression. This will provide an effective ultrahigh Q factor (and hence optical linewidth) and low residual timing and amplitude noise.

References for Section 1

1. P. J. Delfyett, D. H. Hartman, and S. Z. Ahmad, "Optical Clock Distribution Using a Mode-Locked Semiconductor Laser Diode System", *IEEE J. Lightwave Technol.* **9**, 1646-1649 (1991).
2. C. Baringer, J. F. Jensen, L. Burns, and R. H. Walden, "A 3-bit, 8 GSPS Flash ADC," *Proc. Indium Phos. Rel. Mater. Conf. 1996* (Institute of Electrical and Electronics Engineers, New York, 1996), p.64-67.
3. P. Xiao, K. Jenkins, M. Soyuer, H. Ainspan, J. Burghartz, H. Shin, M. Dolan, D. Harame, "A 4b 8GSample/s A/D Converter in SiGe Bipolar Technology", *Proc. IEEE Intl. Solid-State Circ. Conf. 1997* (Institute of Electrical and Electronics Engineers, New York, 1997), p.124-125.
4. S. B. Kaplan, P. D. Bradley, D. K. Brock, D. Gaidarenko, D. Gupta, W. Li, and S. V. Rylov, "A Superconductive Flash Digitizer with On-Chip Memory", *IEEE Trans. Appl. Superconduct.* **9**, p. 3020-3025 (1999).
5. D. H. Auston, "Picosecond optoelectronic switching and gating in silicon", *Appl. Phys. Lett.* **26**, p.101-103 (1975).
6. H. F. Taylor, "An Optical Analog-to-Digital Converter—Design and Analysis", *IEEE J. Quantum Electron.* **QE-15**, p. 210-216 (1979).
7. J. A. Valdmanis, G. Mourou, and C. W. Gabel, "Picosecond electro-optic sampling system", *Appl. Phys. Lett.* **41**, p. 211-212 (1982).
8. R. A. Becker, C. E. Woodward, F. J. Leonberger, and R. C. Williamson, "Wide-band electrooptic guided-wave analog-to-digital converters", *Proc. IEEE* **72**, p. 802-819 (1984).
9. T. Kanada and D. L. Franzen, "Optical waveform measurement by optical sampling with a mode-locked laser diode", *Opt. Lett.* **11**, p. 4-6 (1986).
10. P. E. Pace, S. J. Ying, J. P. Powers, and R. J. Pieper, "Integrated optical sigma-delta modulators", *Opt. Eng.* **35**, p. 1828-1836 (1996).
11. T. R. Clark, J. U. Kang, and R. D. Esman, "Performance of a Time- and Wavelength-Interleaved Photonic Sampler for Analog-Digital Conversion", *IEEE Photon. Technol. Lett.* **11**, p. 1168-1170 (1999).
12. Johnstone, M. F. Lewis, J. D. Hares, and P. A. Kellett, "High-speed opto-electronic transient waveform digitizer", Third Int'l Conf. on Advanced A/D and D/A Convrsn Techniques and their Applications 1999, (Institute of Electrical and Electronics Engineers, New York, 1999), p. 21-24.
13. E. N. Toughlian and H. Zmuda, "A photonic wide-band analog to digital converter", *Int'l Topical Meeting on Microwave Photonics* p. 248-250 (2000).
14. S. Bhushan, P. Kelkar, and B. Jalali, "30 Gsample/s time-stretch analogue-to-digital converter", *Electron. Lett.* **36**, p. 1526-1527 (2000).
15. P. Rabiei and A. F. J. Levi, "Analysis of Hybrid Optoelectronic WDM ADC", *IEEE J. Lightwave Technol.* **18**, p. 1264-1270 (2000).
16. M. Johansson, B. Löfving, S. Hård, L. Thylén, M. Mokhtari, U. Westergren, and C. Pala, "Study of an ultrafast analog-to-digital conversion scheme based on diffractive optics", *Appl. Opt.* **39**, p. 2881-2887 (2000).

17. R. H. Walden, "Analog-to-digital converter survey and analysis", *IEEE J. Select. Areas Commun.* **17**, p. 539-550 (1999).

18. H. Shi, J. Finlay, G. A. Alphonse, J. C. Connolly, and P. J. Delfyett, "Multiwavelength 10-GHz picosecond pulse generation from a single-stripe semiconductor diode laser", *IEEE Photon. Technol. Lett.* **9**, p. 1439-1441 (1997).

19. E. Park, P. J. Delfyett, and J. H. Abeles, "Multi-wavelength generation at 1.55 μm from an external cavity semiconductor laser", *Proc. SPIE*, **4042**, p. 82-90 (2000).

20. H. Shi, I. Nitta, G. A. Alphonse, J. C. Connolly, and P. J. Delfyett, "Timing Jitter Performance of Multiwavelength Modelocked Semiconductor Laser", *Electron. Lett.* **34**, p. 1-2 (1998).

21. D. J. Derickson, A. Mar, and J. E. Bowers, "Residual and absolute timing jitter in actively modelocked semiconductor lasers", *Electron. Lett.* **26**, p. 2026-2028 (1990).

22. D. von der Linde, "Characterization of the Noise in Continuously Operating Mode-Locked Lasers", *Appl. Phys. B.* **39**, p. 201-217 (1986).

23. P.-T. Ho, "Phase and Amplitude Fluctuations in a Mode-Locked Laser", *IEEE J. Quantum Electron.* **QE-21**, p. 1806-1813 (1985).

24. D. R. Hjelme and A. R. Mickelson, "Theory of Timing Jitter in Actively Mode-Locked Lasers", *IEEE J. Quantum Electron.* **QE-28**, p. 1594-1605 (1992).

25. F. Rana and R. Ram, "Timing Jitter and Noise in Mode-Locked Semiconductor Lasers", *Conference on Electro-Optics and Lasers 2001*, paper CMB2.

26. A. S. Hou, R. S. Tucker, and G. Eisenstein, "Pulse Compression of An Actively Modelocked Diode Laser Using Linear Dispersion in Fiber", *IEEE Photon. Technol. Lett.* **2**, p. 322-324 (1990).

REFERENCES FOR SECTION 2

27. DePriest, C. M., Braun, A., Abeles, J., and Delfyett, Jr. P. J.: '10 GHz Ultralow-noise optical sampling stream from a semiconductor diode ring laser', IEEE Photon. Technol. Lett., to be published.

28. Derickson, D. J., Mar, A., and Bowers, J. E.: 'Residual and absolute timing jitter in actively modelocked semiconductor lasers', Electron. Lett., 1990, 26, (24), pp. 2026-2028.

29. Clark, T. R., Carruthers, T. F., Matthews, P. J., and Duling III, I. N.: 'Phase noise measurements of ultrastable 10 GHz harmonically modelocked fibre laser', Electron. Lett., 1999, 35, (9), pp. 720-721.

30. Ng, W., Stephens, R., Persechini, D., and Reddy, K. V.: 'Ultra-low jitter modelocking of Er-fibre laser at 10 GHz and its application in photonic sampling for analogue-to-digital conversion', Electron. Lett., 2001, 37, (2), pp. 113-115.

31. Walden, R. H.: 'Analog-to-digital converter survey and analysis', IEEE J. Select. Areas in Commun., 1999, 17, (4), pp. 539-550.

32. Nelson, C., Walls, F. L., and Boggs, C. K.: 'Extending the range for precision AM noise measurements', IEEE Freq. Control. Symp., 1996, pp. 854-857.

33. Hjelme, D. R. and Michelson, A. R.: 'Theory of timing jitter in actively mode-locked lasers', IEEE J. Quantum Electron., 1992, 28, (6), pp. 1594-1606.

34. Rana, F. and Ram R.: 'Noise and timing jitter in active and hybrid mode-locked semiconductor lasers', CLEO, 2001, pp. 6-7.

35. Von der Linde, D.: 'Characterization of the noise in continuously operating mode-locked lasers', Appl. Phys. B, 1986, 39, pp. 201-217.

REFERENCES FOR SECTION 3

36. G. T. Harvey, L. F. Mollenauer, "Harmonically mode-locked fiber ring laser with an internal Fabry-Perot stabilizer for soliton transmission", Opt. Lett. **18**, 107 (1993).
37. T. Yilmaz, C. M. DePriest, P. J. Delfyett, Jr., "Complete noise characterization of an external-cavity semiconductor laser hybridly modelocked at 10 GHz", *Electron. Lett.* accepted for publication.
38. D. J. Derickson, A. Mar, and J. E. Bowers, "Residual and absolute timing jitter in actively modelocked semiconductor lasers", *Electron. Lett.*, **26**, 2026 (1990).
39. J. S. Wey, J. Goldhar, G. L. Burdge, "Active harmonic modelocking of an erbium fiber laser with intracavity Fabry-Perot filters", *J. Lightwave Technol.* 15, 1171 (1997).

REFERENCES FOR SECTION 4

40. C. M. DePriest, A. Braun, J. H. Abeles, and P. J. Delfyett, Jr., "10-GHz ultra-low noise optical sampling stream from a semiconductor diode ring laser," IEEE Photonics Technol. Lett. **13**, 1109-1111 (2001).
41. D. J. Derickson, A. Mar, and J. E. Bowers, "Residual and absolute timing jitter in actively modelocked semiconductor lasers," Electron. Lett. **26**, 2026-2028 (1990).
42. T. Yilmaz, C. M. DePriest, and P. J. Delfyett, Jr., "Complete noise characterization of an external cavity semiconductor laser hybridly modelocked at 10 GHz," Electron. Lett. **37**, 1338-1339 (2001).
43. C. M. DePriest, T. Yilmaz, P. J. Delfyett, Jr., School of Optics/CREOL, University of Central Florida, Orlando, FL 32816 are preparing a manuscript to be called "Ultralow noise and supermode suppression in an actively-modelocked external-cavity semiconductor diode ring laser."
44. C. H. Henry, "Theory of the linewidth of semiconductor lasers," IEEE J. Quantum Elec. **QE-18**, 259-264, (1982).
45. D. M. Baney and W. V. Sorin, "High resolution optical frequency analysis," in *Fiber Optic Test and Measurement*, D. Derickson, ed. (Prentice Hall PTR, Upper Saddle River, N.J., 1998), pp. 169-219.
46. D. von der Linde, "Characterization of the noise in continuously operating mode-locked lasers," Appl. Phys. B. **39**, 201-217, (1986).
47. D. R. Hjelme and A. R. Mickelson, "Theory of timing jitter in actively modelocked lasers," IEEE J. Quantum Elec. **QE-28**, 1594-1605, (1992).
48. F. Rana and R. Ram, "Timing Jitter and Noise in Mode-Locked Semiconductor Lasers", Conference on Electro-Optics and Lasers 2001, paper CMB2.
49. D. W. Rush, G. L. Burdge, and P. T. Ho, "The linewidth of mode-locked semiconductor laser caused by spontaneous emission: Experimental comparison to single-mode operation," IEEE J. Quantum Elec. **QE-22**, 2088-1091, (1986).